Computational Study on Spatially Distributed Sequential Stimulation for Fatigue Resistant Neuromuscular Electrical Stimulation

Silviu Agotici, Kei Masani, and Paul B. Yoo, *Member, IEEE*

***Abstract*— Neuromuscular electrical stimulation (NMES) is used to artificially induce muscle contractions of paralyzed limbs in individuals with stroke or spinal cord injury, however, the therapeutic efficacy can be significantly limited by rapid fatiguing of the targeted muscle. A unique stimulation method, called spatially distributed sequential stimulation (SDSS), has been shown clinically to reduce fatiguing during FES, but further improvement is needed. The purpose of this study was to gain a better understanding of SDSS-induced neural activation in the human lower leg using a computational approach. We developed a realistic finite element model of the lower leg to investigate SDSS, by solving the electric field generated by SDSS and predicting neural activation. SDSS applied at 10 Hz was further compared with conventional transcutaneous stimulation that delivered electrical pulses at 40 Hz through a single electrode. We found that SDSS electrically activated multiple sub-populations of motor neurons within the TA muscle that fired at frequencies ranging between 10 Hz and 40 Hz. This complex nerve activation pattern depicts the mechanism of action of SDSS for reducing muscle fatigue during NMES.**

***Index Terms*— Neuromuscular electrical stimulation, fatigue, spatially distributed sequential stimulation, finite element analysis.**

I. Introduction

TRANSCUTANEOUS neuromuscular electrical stimulation (NMES) is used to artificially activate nervous tissue by applying short electric impulses at the surface of the skin. When NMES is used to generate functional movements by temporally sequencing muscle contractions, it is commonly referred to as functional electrical stimulation (FES). Individuals with spinal cord injury or stroke can be helped through FES, which specifically targets peripheral nerves to rehabilitate motor functions. FES was originally developed as a neuroprosthetic system aimed at assisting the users' daily-life activities, while, more recently, the same technology is being implemented as a short-term clinical intervention (FES therapy) to help individuals regain or improve upper and lower extremity functions [1], [2]. Existing clinical data suggests that FES can significantly help individuals with neurological disorders [3]; however, stimulation-evoked fatigue is recognized as a major clinical limitation.

Restoration of lower extremity function by means of NMES can be achieved through activation of lower motor neurons (LMNs) located beneath surface electrodes placed in close proximity to target nerve processes [4]. But, rapid onset of muscle fatigue is a well-documented phenomenon that results from non-physiological recruitment of peripheral nerve fibers [4]–[7], where larger diameter myelinated fibers are electrically recruited at lower stimulation amplitudes than smaller diameter fibers. And unlike the physiological activation of muscle units, electrical pulses synchronously and repeatedly activate the same, local population of motor units, generating synchronous activation of muscle fiber contractions such as the case when NMES is applied via a conventional, single electrode stimulation (SES) approach [3]. Rapid muscle fatigue is often compounded by the fact that muscle fibers of individuals with neurological disorders have undergone changes in metabolic function – shift to fast fatiguing muscle fibers [7], [8].

As a potential solution aimed at circumventing this problem, a unique NMES approach called Spatially Distributed Sequential Stimulation (SDSS) has been investigated, where multiple stimulation channels are used in sequential manner to activate different subcomponents of a target muscle [6], [9]–[18]. That is, while SES uses a single cathode with a certain stimulation frequency (e.g., 40 Hz), SDSS uses multiple active electrodes that are sequentially stimulated at a fractionally lower stimulation frequency (e.g., 10 Hz), in which the local population of activated motor units are distributed both spatially and temporally. Early feasibility studies have shown improvements in muscle fatigue characteristics, but further development of SDSS is needed to facilitate clinical translation [3], [6]. To this end, a better understanding of the mechanism underlying SDSS is needed to further

Manuscript received September 17, 2020; revised February 12, 2021; accepted March 17, 2021. Date of publication December 6, 2021; date of current version December 21, 2021. This work was supported in part by the Canadian Institutes of Health Research under Grant PJT148851 and in part by the Canada Foundation for Innovation (CFI) through a Leaders Opportunity Fund under Grant 31506. *(Corresponding author: Paul B. Yoo.)*

Silviu Agotici is with the Institute of Biomedical Engineering, University of Toronto, Toronto, ON M5S 3G9, Canada (e-mail: silviu.agotici@mail.utoronto.ca).

Kei Masani is with the KITE, Toronto Rehabilitation Institute—University Health Network, Toronto, ON M4G 3V9, Canada, and also with the Institute of Biomedical Engineering, University of Toronto, Toronto, ON M5S 3G9, Canada (e-mail: k.masani@utoronto.ca).

Paul B. Yoo is with the Institute of Biomedical Engineering (BME) and Edward E. Rogers Department of Electrical and Computer Engineering (ECE), University of Toronto, Toronto, ON M5S 3G9, Canada (e-mail: paul.yoo@utoronto.ca).

Digital Object Identifier 10.1109/TNSRE.2021.3133508

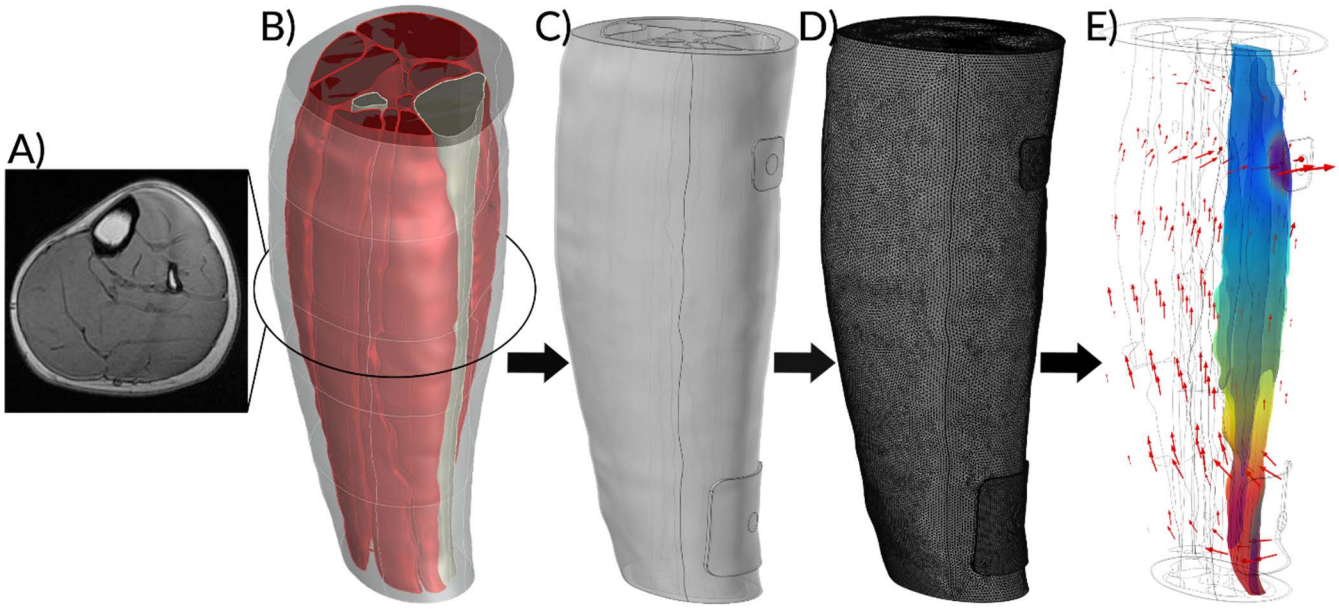

Fig. 1. Overview of the framework used in the computational study. A) Preparation of sequential MRI images of a human lower leg. B) Development of realistic 3D model within Autodesk Inventor. C) Import 3D model into Comsol Multiphysics using LiveLink for Inventor and add additional geometry, set electrical properties boundary conditions. D) Meshing of the FEM and E) solve for electric potential of the FEM. The electric potential (surface plot) and current density (arrows) are displayed for the TA muscle.

develop this NMES technique in a clinically meaningful manner.

The goal of this study was to create a realistic computational model of the human lower leg and characterize the specific nerve activation patterns that link SDSS to reduced muscle fatigue. We hypothesized that the fatigue-resistant properties of SDSS are due to its ability to activate multiple groups of LMNs at varying stimulation frequencies. The complex pattern of neural activation was investigated computationally by analyzing and comparing the electrical activation of the tibialis anterior (TA) muscle using SES and SDSS electrode configurations.

II. Methods

A realistic computational model was created via a 3D finite element model (FEM) derived from a dataset of Magnetic Resonance Imaging (MRI) images (Figure 1). The model of the human lower leg was initially constructed using Autodesk Inventor 2019 (San Rafael, CA, USA) and subsequently imported into the FEM software environment (Comsol Multiphysics v5.3a, Comsol Inc., Burlington, MA, USA). The FEM solved the electrical potentials generated by a NMES current and was subsequently used to predict neural activation in Matlab environment (ver. R2018a, MathWorks Incorporated, Natick, MA, USA).

A. Finite Element Model

Autodesk Inventor was used to manually segment and loft through a series of MRI images (8 mm spacing between slices) to create a 3D model of an adult lower leg (Figure 1A & B). The model was imported into Comsol Multiphysics via Livelink for Inventor (Comsol Inc). Livelink for Inventor was used to edit, add, or remove objects from the 3D model, where changes were automatically transferred to the FEM in Comsol (Figure 1C). Within the FEM environment, additional objects such as skin (1.39 mm thickness), surface electrodes (4.5 mm thickness) and nerves were added. Each electrode consisted of three layers: stainless-steel contact (thickness = 1 mm), gel layer (1 mm), and a rubber layer (2.5 mm). The dimensions and electrical conductivity values were matched to the type C electrode in Saturnino *et al.* [22]. The electrical conductivity of each object was assigned (Table I), boundary conditions were defined, and the model was meshed (Figure 1D). The resulting electric fields (Figure 1E) were subsequently exported using Livelink for Matlab.

TABLE I
Electrical Conductivity of Materials Used in FEMs [19]–[22]

Material	Electrical Conductivity (S/m)
Skin	0.0014
Fat	0.03
Connective Tissue	0.15
Bone	0.02
Radial Muscle	0.11
Axial Muscle	0.33
Radial Endoneurium	0.0826
Axial Endoneurium	0.517
Perineurium	0.0021
Epineurium	0.0826
Stainless-Steel	74×10^5
Rubber Pad	0.1
Conductive Gel	4

SES was modeled using a 5 × 5 cm cathodic electrode placed above the TA muscle belly, with the center of the electrode positioned 7 cm below the tibial tuberosity and the medial edge positioned 1 cm medial to the tibial crest (Figure 2). SDSS was implemented by dividing the SES

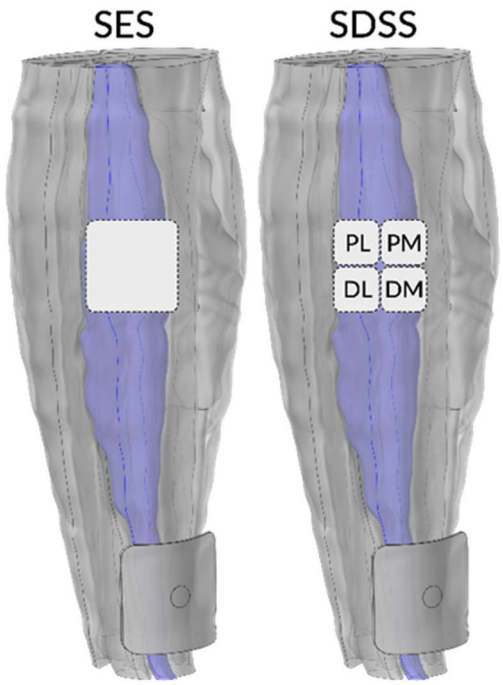

Fig. 2. Cathode (white) and anode (gray) electrode placement for Single Electrical Stimulation (SES) and Spatially Distributed Sequential Stimulation (SDSS) configurations on the right lower leg, with the Tibialis Anterior (TA) muscle in blue. The SES is composed of a single active cathode (white electrode); whereas the SDSS involves 4 independent cathodes (white electrodes), labeled according to orientation on the leg surface over the TA muscle (Proximal Lateral (PL), Proximal Medial (PM), Distal Lateral (DL), and Distal Medial (DM)).

electrode into four individual electrodes (2.5 × 2.5 cm), that were labeled as proximal-lateral (PL), proximal-medial (PM), distal-lateral (DL), and distal-medial (DM). In both models, the return electrode (e.g., anode of SES) was centered 7 cm proximal from the medial malleolus, directly over the tibial crest.

Simulations were performed by applying a current through a SES or SDSS electrode at different amplitudes (15 mA – 60 mA) and polarities (cathodic and anodic stimulation). The steady-state current used in this model (AC/DC solver, COMSOL Multiphysics) was used to approximate monophasic stimulus pulses. Each simulation required approximately 15 minutes to complete. The volumetric electric potential data were extracted for the TA and surrounding muscles, with 1 mm sampling interval used in all 3 directions. Computations were performed with a DELL Precision T5600 Workstation (Intel Xeon E52630 2.3 GHz processor, 64 GB RAM).

B. Estimation of Nerve Activation

The extracellular electric potential data imported into Matlab were formatted as multiple horizontal data planes separated by 1 mm intervals. Within each plane, data points were sampled at 1 mm intervals in both the x- and y-directions. The 1 mm interval corresponded to the distance between nodes of Ranvier of 10 μm motor neurons, which were assumed to be uniformly distributed throughout muscle tissue. The 1 mm spacing was determined by solving for L, using the relationship L/D = 100, where D is the diameter of a myelinated axon (10 μm) and L is the internodal distance between nodes of Ranvier [23]. Neural activation was predicted by calculating the activating function (AF), which is defined by the second spatial difference of the extracellular voltage along 3 successive nodes of Ranvier [24].

III. Data Analysis

A. Defining Nerve Fibers Within the Muscle

The number of unique nerve fibers located within the TA muscle was defined by the 1 mm sampling distance of adjacent nodes of Ranvier. Nerve fibers oriented in the lateral-medial direction (x-direction) passed through the sagittal plane and fibers oriented in the anterior-posterior direction (y-direction) passed through the coronal plane. Transverse fibers were oriented in the superior-inferior direction (z-direction). We assumed that fibers in the x- and y-direction spanned across the muscle without branching. In contrast, z-direction fibers were constructed to mimic the innervation pattern of tibial nerve branches that project to different segments along the length of the TA muscle. We assumed that individual fibers did not extend along the entire longitudinal (z-direction) length of the TA muscle. Instead, z-direction motor fibers were modeled as 20 mm long segments that were stacked in longitudinal fashion. An LMN was classified as being electrically activated if the AF of any node of Ranvier along the nerve fiber exceeded a predetermined threshold value (see below).

B. Thresholding of the Activating Function

The AF provides a relative measure of neural excitability, which can allow a quantitative comparison of neuromuscular activation between different methods of electrical stimulation [25]. In this study, we compared the activation properties of the TA muscle between SES and SDSS electrodes by first defining the AF values that correspond to the activation thresholds of the TA muscle for each electrode type. Using COMSOL, we computed the AF value at which a 15 mA current pulse yielded an approximately 10% activation of total LMNs. These criteria were set to be consistent with typical TA muscle activation thresholds measured in humans [13]. Analysis of percent activation of the TA using a weighted average approach (described in Figure 4) yielded a threshold AF of 0.002 (10.6% activation of TA) for SES; and a threshold of 0.0017 (9.7% activation of TA) for SDSS electrodes. The minor difference in thresholds did not affect the overall results of this study.

C. Analysis of Stimulation Overlap

The extent of electrically activating independent subsets of nerve fibers by SDSS was assessed by stimulation overlap, which relates to the degree of fatigue resistance provided by SDSS. In addition to analyzing the percentage of LMNs that were activated by pairs of SDSS electrodes, we calculated the proportion of LMNs that were uniquely or repeatedly activated by the four SDSS electrodes through which stimulation pulses

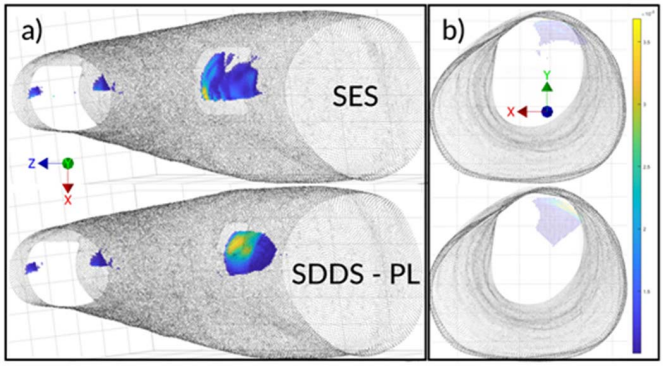

Fig. 3. Sample volumetric plot of the activating function (AF) for nerve fibers oriented in the z-direction (longitudinal), where electrical stimulation (15 mA) was applied using SES or SDSS (PL electrode). The AF plots are shown from (a) anterior and (b) rostral viewpoints.

were applied in sequential manner (e.g., PL–PM–DM–DL). We used a sequential stimulation frequency of 10 Hz, such that LMNs could be activated at frequencies between 10 Hz and 40 Hz. Electrical stimulation at a frequency of 40 Hz indicated the same LMNs were activated by all 4 electrodes during each cycle through the SDSS array. Overlapped activation of different LMNs (x, y, z orientated fibers) was analyzed by creating 2-dimensional projection plots of the total cumulative number of times each LMN type was activated by SDSS. LMNs oriented in the x, y, and z directions were plotted as a projection onto the sagittal, coronal, and transverse planes of the leg, respectively.

IV. Results

The FEM enabled characterization of nerve fiber activation within the TA muscle. As an example (Figure 3), a comparison between the SES and SDSS electrodes showed that the volume of electrically activated (z-direction) nerve fibers was notably smaller for the SDSS electrode. In particular, the depth of LMNs within the TA that were activated by the SDSS electrode was about 2 times greater than that of the SES electrode.

A. TA Percent Activation for SDSS and SES

Although electrical stimulation at 15 mA yielded comparable recruitment of LMNs between SES (9.7%) and SDSS (10.6%) electrodes (weighted average data, Figure 4D), recruitment of LMNs at higher stimulation amplitudes ($\geq$30 mA) was notably greater for the SES electrode (range = 27.7% to 38.5%). As depicted in Figure 4A & 4C, this was particularly evident for x- (SDSS = 17.3% to 38.1% vs. SES = 24.6% to 43.9%) and z-direction fibers (SDSS = 23.1% to 32.8% vs. SES = 40.8% to 49.1%), which showed that the larger SES electrode was more effective at recruiting LMNs than a single SDSS electrode. A similar trend was observed for y-direction fibers (Figure 4B), but overall recruitment of these fibers was smaller for both SES and SDSS electrodes.

B. SDSS Percent Overlap

The average % activation of LMNs achieved by individual SDSS electrodes was compared to those that were co-activated (i.e., overlap) by pairs of SDSS electrodes (Figure 5). In both cases, there was a gradual increase in recruitment of LMNs as the stimulus amplitude was increased. Consistent with Figure 4, electrical recruitment of y-direction LMNs was comparatively poor. Between 15 mA and 60 mA, the % activation of LMNs (weighted average) by SDSS electrodes ranged from 11% to 27% (Figure 5A); whereas the percentage of overlapped LMNs was approximately half (6% to 17%) of those activated by only one SDSS electrode (Figure 5B).

C. Cathodic SDSS Stimulation

At stimulation threshold (Figure 6A-B), x- and y-direction fibers activated by 1 or 2 SDSS electrodes were primarily located along the outer boundary of the SDSS array; whereas the population of fibers activated by 3 or more electrodes were located near the center of the array. In the transverse projection of z-direction fibers (Figure 6C), LMNs activated by 3 or more SDSS electrodes are located within a central region beneath the skin surface; whereas LMNs activated by 1 or 2 electrodes are located outside this region. As shown in Figure 7, the percent activation of both unique and overlapped LMNs increased with stimulation amplitude. As the amplitude reached 60 mA, x-direction fibers exhibited marked increases in the percentage of LMNs activated by 3 or more electrodes, while y-directed fibers exhibited notable increases in LMNs activated by 1 or 2 electrodes. On the other hand, z-direction fibers exhibited an increase in overlapped fiber activation by 2 and 4 SDSS electrodes (Figure 7C). It is noted that at 30 mA, there were very few nerve fibers activated by 1 or 3 SDSS electrodes.

D. Anodic SDSS Stimulation

Compared to cathodic stimulation, anodic SDSS showed a notably different pattern in the electrical recruitment of y- and z-direction fibers. As illustrated in Figure 8B-C, there were markedly larger areas that corresponded to LMN activation by 1 or 2 SDSS electrodes. As a result, the regions delineating LMNs activated by 4 electrodes (yellow region) were virtually absent or significantly reduced for y- and z-fibers, respectively. These patterns were confirmed when comparing the percent activation of TA fibers (Figure 9B-C). In contrast, electrical activation of LMNs oriented in the x-direction was similar to that of cathodic stimulation (Figure 8A), where LMN activation by 4 SDSS electrodes exhibited the highest rate of increase as the stimulation amplitude was increased (Figure 9A).

E. Differential LMN Activation (SES Vs. SDSS)

As illustrated in Figure 10, cathodic SDSS stimulation consistently resulted in the electrical activation of more LMNs (i.e. total axons) than that achieved by the single SES electrode. At 15 mA, SDSS (24% activation) exhibited a 2.2-fold greater activation of LMNs over SES (11% activation). And at higher amplitudes, the difference in TA % activation was smaller between SDSS and SES configurations, ranging between 6% and 8%.

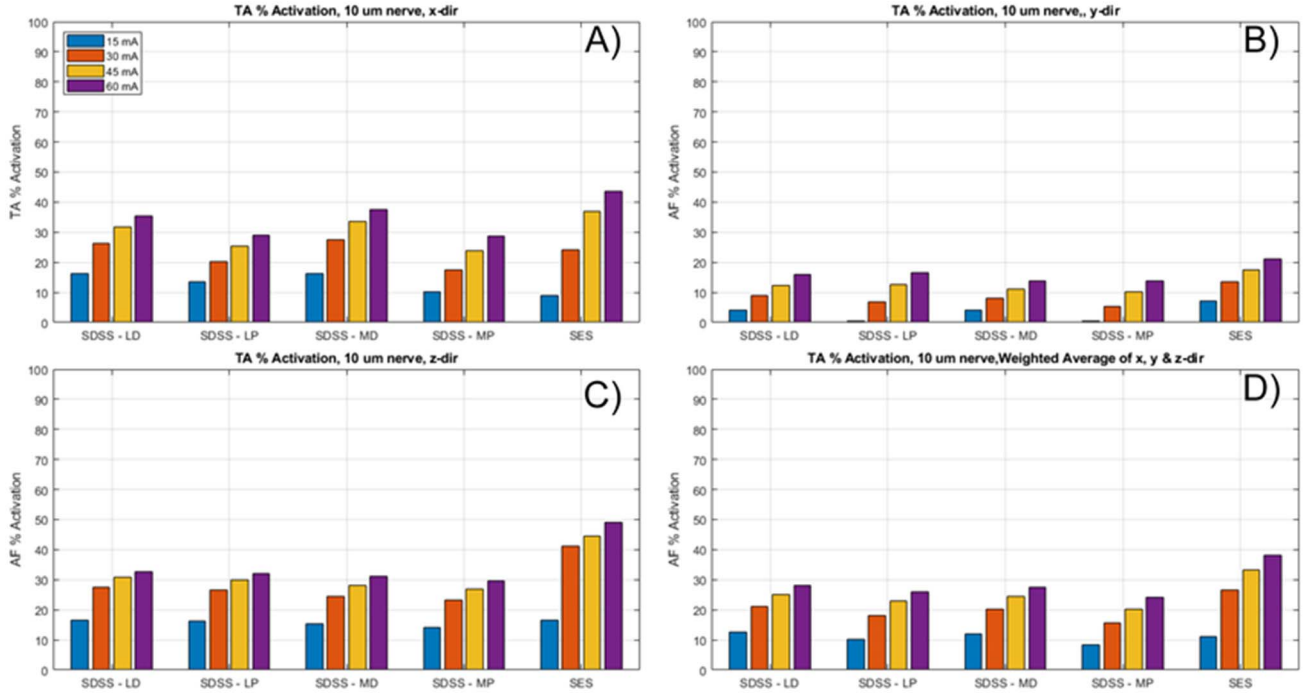

Fig. 4. Comparison of percent (%) activation of the TA among SDSS (LD, LP, MD, and MP) and SES electrodes, which were used to simulate NMES at different stimulation amplitudes (10 mA to 60 mA). The % activation was plotted for (A) x-, (B) y-, (C) z-directions and for (D) the weighted average, which was calculated by summing the total number of activated LMNs in the x, y, and z directions and dividing this value by the total number of LMNs in all 3 directions.

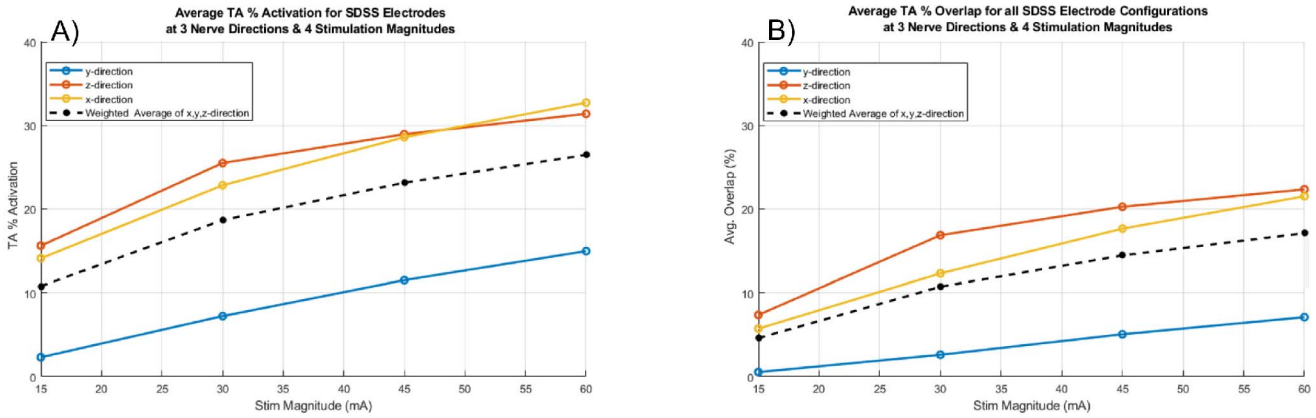

Fig. 5. Analysis of (A) individual and (B) overlapped activation of TA fibers achieved by pairs of SDSS electrodes. Data were represented as percent activation of LMNs averaged across 6 paired combinations of SDSS electrodes (PM, PL, DM, and DL). The % activation data were plotted as a function of stimulation amplitude and divided with respect to fiber orientation (x, y, z, and weighted average).

In conjunction with a greater number of LMNs being activated, SDSS also resulted in groups of LMNs being activated at different frequencies. As an example, Figure 10 showed that cathodic SDSS at 30 mA resulted in 25%, 45%, 10%, and 20% of LMNs being activated by 1 (10 Hz), 2 (20 Hz), 3 (30 Hz) and 4 (40 Hz) of the SDSS electrodes, respectively. The Total axons activated (SDSS) refers to the sum of all 4 groups of LMNs. SDSS resulted in 70% of LMNs being activated at lower frequencies (10 or 20 Hz), which can be thought to contribute to the fatigue-resistive properties of SDSS in human subjects [26].

It is noted that anodic SDSS exhibited a similar pattern of LMN activation to that of cathodic SDSS (data not shown). There was a less than 5% difference in the total number of activated LMNs between anodic and cathodic SDSS. While cathodic stimulation resulted in 4-10% more LMNs being activated at lower frequencies 10 Hz; anodic stimulation exhibited a greater number of LMNs activated at 40 Hz.

V. Discussion

The mechanism by which SDSS can reduce stimulation-induced muscle fatigue during NMES was shown to be

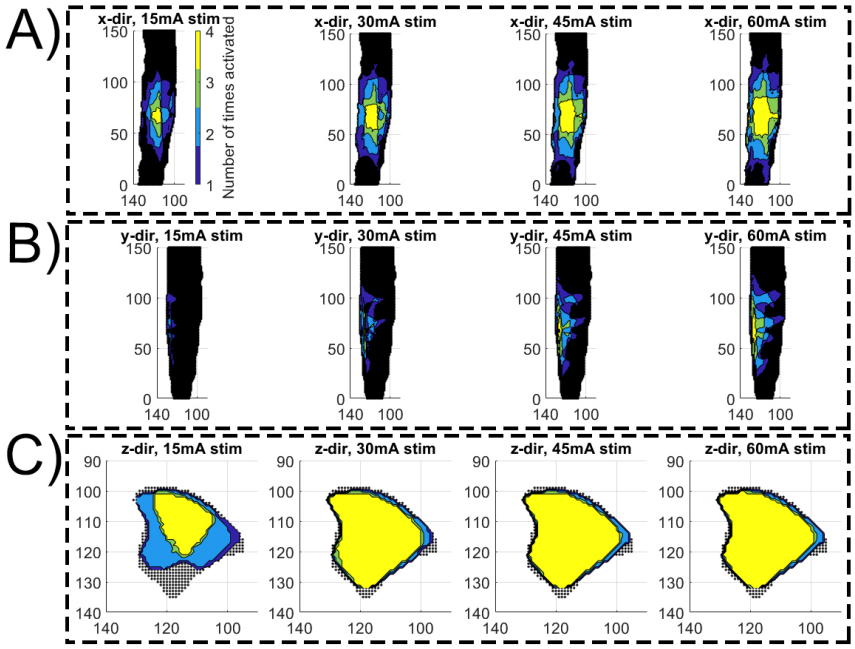

Fig. 6. Images of (A) Sagittal, (B) coronal and (C) transverse projections of LMNs in the TA that were activated by 1, 2, 3, or 4 of the SDSS electrodes during cathodic stimulation. The color map consists of 4 colors (left panel in A) – yellow, green, blue, and purple – that represent motor neurons activated by 4, 3, 2, or 1 of the SDSS electrodes, respectively. SDSS electrode placement is shown in Figure 2.

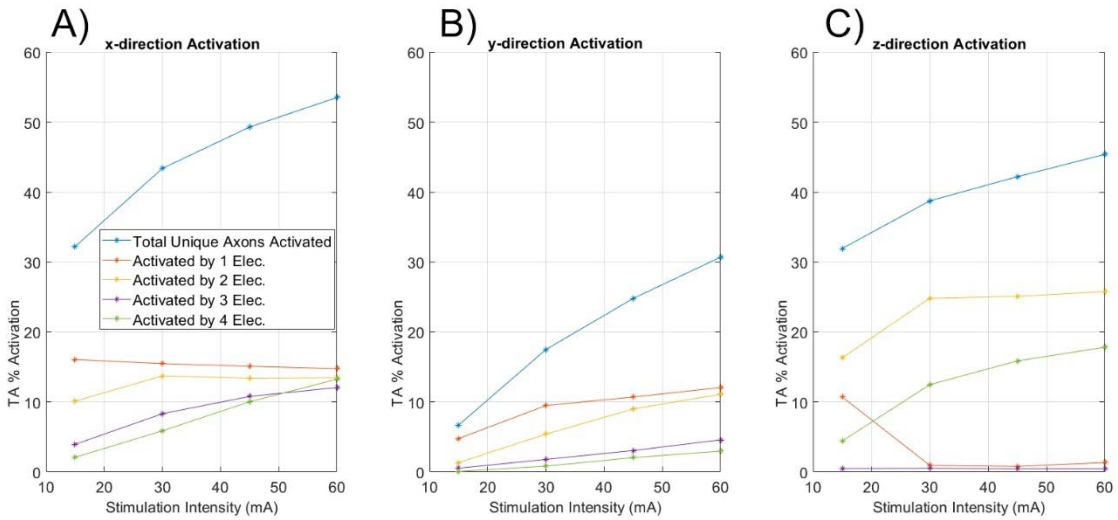

Fig. 7. Summary of the % LMN activation in the TA muscle, oriented in the (A) x-, (B) y-, and (C) z-directions. As the stimulation amplitude was increased between 15 mA and 60 mA, data were plotted for cathodic stimulation corresponding to LMN activation by 1, 2, 3, or 4 SDSS electrodes. The total number of unique LMNs activated by all 4 SDSS electrodes was also plotted.

achieved through the sequential and alternating activation of different subcomponents of excitable tissue (i.e., TA muscle). To achieve this by means of NMES, our results showed that multiple electrodes were needed to stimulate nerve fibers in distributed fashion. It is further noted that the majority of LMNs activated by SDSS were stimulated at frequencies (10 and 20 Hz) known to be less prone to muscle fatigue. In general, SDSS requires an array of surface electrodes that have a smaller surface area than that of a single SES electrode [6], [9]–[14]. For the purpose of electrically activating the same target muscle in this computational study, we modeled the SDSS array to consist of electrodes that were 1/4th the size of a single SES patch typically used to stimulate the human TA muscle [6], [9]–[12], [14]. When compared to SES, our simulations showed that each individual SDSS electrode activated a smaller volume of excitable tissue (%TA activation, Figure 4). Interestingly, however, we found that the smaller SDSS electrodes achieved not only more regionally selective activation of excitable tissue but that nerve fibers located deeper within the TA muscle were also recruited by the SDSS electrodes (Figure 3). The combined total number of unique LMNs activated by SDSS was on average 7.9 percentage

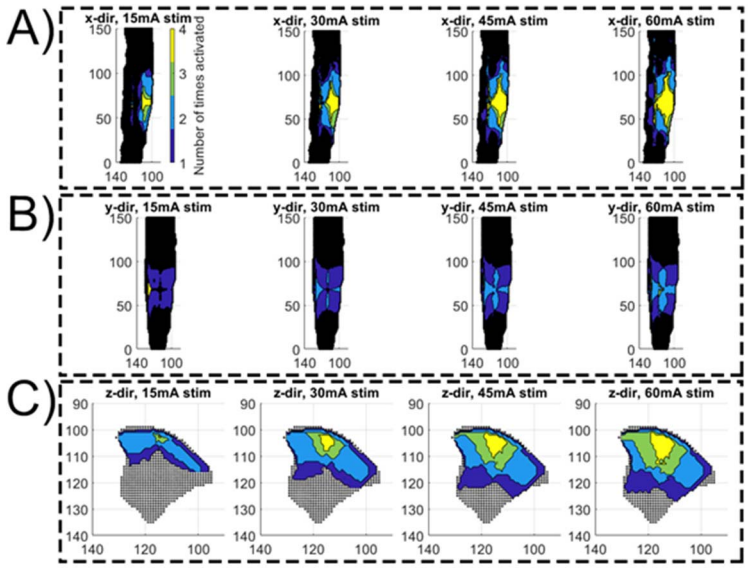

Fig. 8. Images of (A) Sagittal, (B) coronal and (C) transverse projections of LMNs in the TA that were activated by 1, 2, 3, or 4 of the SDSS electrodes during anodic stimulation. The color map consists of 4 colors (left panel in A) – yellow, green, blue, and purple – that represent motor neurons activated by 4, 3, 2, or 1 of the SDSS electrodes, respectively. SDSS electrode placement is shown in Figure 2.

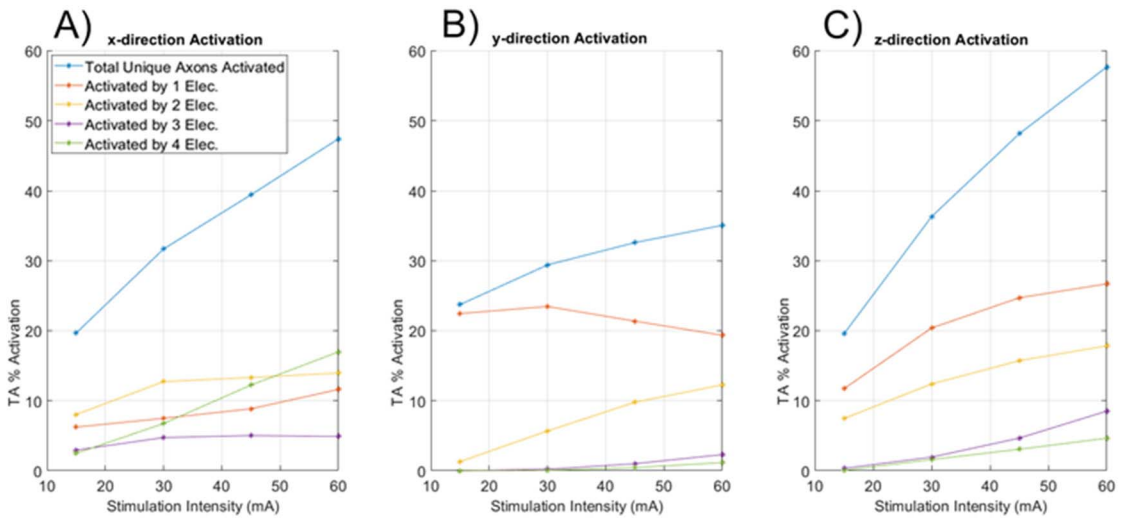

Fig. 9. Summary of the % LMN activation in the TA muscle, oriented in the (A) x, (B) y, and (C) z directions. As the stimulation amplitude was increased between 15 mA and 60 mA, data were plotted for anodic stimulation corresponding to LMN activation by 1, 2, 3, or 4 SDSS electrodes. The total number of unique LMNs activated by all 4 SDSS electrodes was also plotted.

points greater than the total activated by SES (Figure 10), which suggested the deeper LMNs activated by SDSS played an important role. As a result, part of the fatigue-resistant properties of SDSS can be attributed to the larger volume of nerve fibers activated by the smaller electrodes – albeit with greater probability of eliciting stimulation-evoked discomfort linked to higher charge density at the skin surface [14].

Next, we examined the extent of repeated activation of individual LMNs that resulted from simulating electrical pulses sequentially delivered through pairs of SDSS electrodes. This was referred to as overlapped stimulation. By increasing the stimulation intensity, we observed an increase in the total number of activated nerve fibers along with a greater number of fibers that exhibited overlapped stimulation (Figure 5B and Figure 6). As one would expect, overlapped stimulation was relatively common for LMNs running in the z- and x-directions, given their parallel orientation with respect to the electrode surface (Figure 6A, C). In contrast, nerve fibers oriented orthogonal to the electrode surface (y-direction) showed markedly lower levels of overlapped stimulation. Also, overlapped stimulation occurred, on average, in 40-60% of LMNs (depending on stimulation intensity) that exhibited co-activation by any pair of the SDSS electrodes (Figure 5A-B).

A consequence of overlapped stimulation is that individual LMNs can become electrically activated at different frequencies, depending on the number of SDSS electrodes that can recruit a particular nerve. In our computational model,

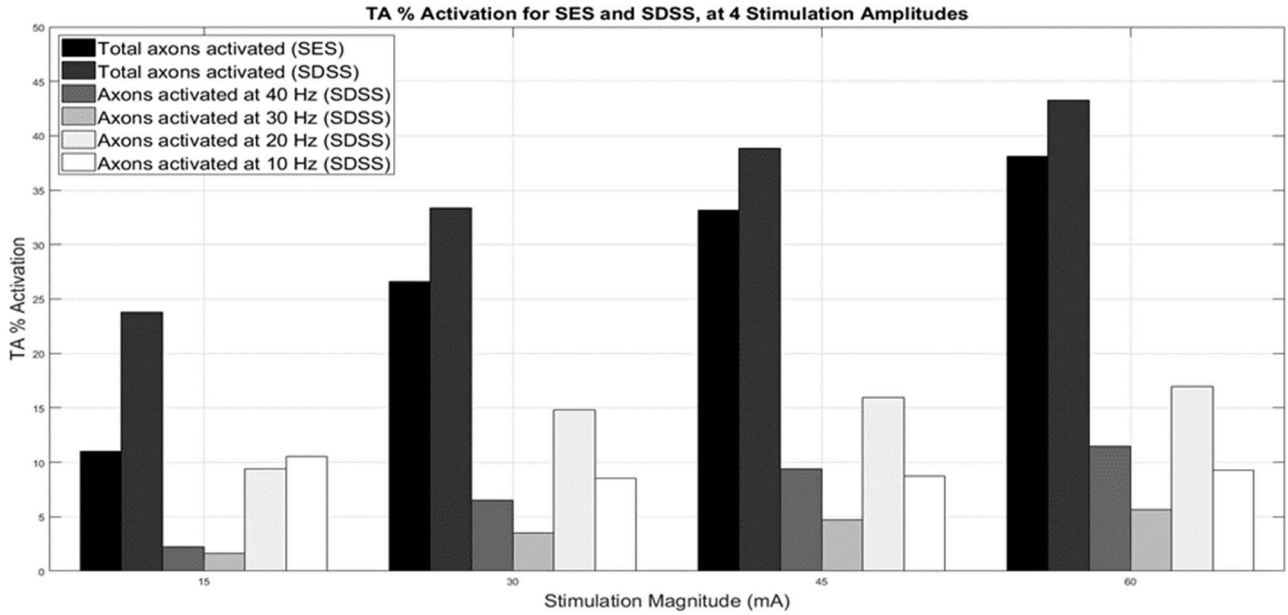

Fig. 10. TA percent activation of all uniquely activated LMNs in cathodal SES and SDSS, and LMNs that were activated at 10, 20, 30, and 40 Hz during cathodal SDSS. The first 2 columns show the percent of total axons that are activated by SES and SDSS, respectively. The remaining 4 columns represent LMNs activated by SDSS electrodes at different stimulation frequencies.

each electrode provided cathodic stimulation at a frequency of 10 Hz, which resulted in individual LMNs firing at a rate between 10 Hz and 40 Hz. Understanding overlapped stimulation within a volume of excitable nervous tissue, irrespective of the sequential order of stimulation among the 4 electrodes, was considered important in understanding SDSS activation. As shown in Figure 10, low-frequency activation of LMNs accounted for over 50% of the total activated fibers and was consequently considered as another key factor contributing to the fatigue-resistant properties of SDSS. High frequency activation of x- and z-direction LMNs (i.e., 40 Hz) were found to primarily occur near the center of the SDSS array, with the degree of overlap becoming weaker as LMNs were located further away from the center point. It is noted that the widespread activation of longitudinal LMNs at 40 Hz depicted in Figure 6C – especially at stimulation intensities >15 mA – was a result of electrically activated LMNs located along the margin between the two proximal and two distal SDSS electrodes. Interestingly, we observed predominant activation of y-direction fibers occurring near the tibial crest (towards the medial side of the TA muscle, Figure 6B). Analysis of current density plots (data not shown) explains this phenomenon by large portions of the stimulus current entering the leg between the TA muscle and the tibia, in a direction perpendicular to the y-direction LMNs.

Previous work by Wonsarnpigoon et al suggests that anodal stimulation can improve the electrical recruitment of axonal processes oriented orthogonal to the surface of an active electrode (i.e., y-direction LMNs), when compared to cathodal stimulation [27]. To this end, we examined anodal SDSS in our model and found that (1) y-direction LMNs exhibited lower activation thresholds compared to cathodic stimulation (Figure 9B vs. Figure 7B) and (2) anodic stimulation achieved more spatially selective activation of y-direction LMNs, as indicated by the larger number of these fibers being activated at lower frequencies ($\leq$20 Hz, Figure 8B). Although these results suggest that fatigue reduction may be further improved by anodal stimulation, further work is needed to determine whether anodal stimulation can achieve comparable torque to that of cathodic stimulation and also confirm the anatomical importance of y-direction fibers.

When compared to SES at the same stimulation intensity, we predict that SDSS will exhibit a decrease in torque due to $\sim$70% of LMNs being activated at lower frequencies of 10 or 20 Hz (Figure 10). But we also expect SDSS to activate more LMNs located further away from the skin surface, which might offset any loss of torque, as our previous comparison of SES vs. SDSS showed no difference in torque output in human participants [13], [26]. SDSS exhibits a lower maximal-tolerated isokinetic torque than what is seen in SES [26], suggesting that individually adjusting the stimulation amplitude of each SDSS electrode and modifying their order of activation may help improve the fatigue-resistant properties.

VI. Conclusion

In this study, we constructed a realistic FEM of the human lower leg that was used to compare the electrical activation of LMNs in the TA muscle. Compared to SES, we discovered that SDSS electrically activated a larger population of LMNs that were located deeper within the TA muscle. Our simulations also showed that SDSS was activating a large proportion of LMNs at frequencies below tetanic muscle contractions. While this is the first computational study to characterize the hypothesized fatigue-resistant mechanisms of SDSS, further work is needed to validate our findings.

ACKNOWLEDGMENT

The authors would like to thank Drs. Yasuo Kawakami and Takaki Yamagishi (Waseda University, Saitama, Japan) for providing the MRI dataset that was used to create the 3D model of the lower leg.

REFERENCES

[1] M. B. Popovic, D. B. Popovic, T. Sinkjær, A. Stefanovic, and L. Schwirtlich, "Restitution of reaching and grasping promoted by functional electrical therapy," *Artif. Organs*, vol. 26, no. 3, pp. 271–275, Mar. 2002.

[2] M. R. Popovic, K. Masani, and S. Micera, "Functional electrical stimulation therapy: Recovery of function following spinal cord injury and stroke," in *Neurorehabilitation Technology*, D. Reinkensmeyer and V. Dietz, Eds. Cham, Switzerland: Springer, 2016, doi: 10.1007/978-3-319-28603-7_25.

[3] K. Masani and M. R. Popovic, "Functional electrical stimulation in rehabilitation and neurorehabilitation," in *Springer Handbook of Medical Technology* (Springer Handbooks), R. Kramme, K. P. Hoffmann, and R. S. Pozos, Eds. Berlin, Germany: Springer, 2011, doi: 10.1007/978-3-540-74658-4_44.

[4] P. H. Peckham and J. S. Knutson, "Functional electrical stimulation for neuromuscular applications," *Annu. Rev. Biomed. Eng.*, vol. 7, no. 1, pp. 327–360, Aug. 2005.

[5] K. T. Ragnarsson, "Functional electrical stimulation after spinal cord injury: Current use, therapeutic effects and future directions," *Spinal Cord*, vol. 46, no. 4, pp. 255–274, 2008.

[6] A. J. Bergquist, V. Babbar, S. Ali, M. R. Popovic, and K. Masani, "Fatigue reduction during aggregated and distributed sequential stimulation," *Muscle Nerve*, vol. 56, no. 2, pp. 271–281, Aug. 2017.

[7] L. R. Sheffler and J. Chae, "Neuromuscular electrical stimulation in neurorehabilitation," *Muscle Nerve*, vol. 35, no. 5, pp. 562–590, 2007.

[8] C. K. Thomas, "Fatigue in human thenar muscles paralysed by spinal cord injury," *J. Electromyogr. Kinesiol.*, vol. 7, no. 1, pp. 15–26, 1997.

[9] R. Nguyen, K. Masani, S. Micera, M. Morari, and M. R. Popovic, "Spatially distributed sequential stimulation reduces fatigue in paralyzed triceps surae muscles: A case study," *Artif. Organs*, vol. 35, no. 12, pp. 1174–1180, Dec. 2011.

[10] R. J. Downey, M. J. Bellman, H. Kawai, C. M. Gregory, and W. E. Dixon, "Comparing the induced muscle fatigue between asynchronous and synchronous electrical stimulation in able-bodied and spinal cord injured populations," *IEEE Trans. Neural Syst. Rehabil. Eng.*, vol. 23, no. 6, pp. 964–972, Nov. 2015.

[11] D. G. Sayenko, R. Nguyen, M. R. Popovic, and K. Masani, "Reducing muscle fatigue during transcutaneous neuromuscular electrical stimulation by spatially and sequentially distributing electrical stimulation sources," *Eur. J. Appl. Physiol.*, vol. 114, no. 4, pp. 793–804, Apr. 2014.

[12] D. G. Sayenko, M. R. Popovic, and K. Masani, "Spatially distributed sequential stimulation reduces muscle fatigue during neuromuscular electrical stimulation," in *Proc. 35th Annu. Int. Conf. IEEE Eng. Med. Biol. Soc. (EMBC)*, Jul. 2013, pp. 3614–3617.

[13] D. G. Sayenko, R. Nguyen, T. Hirabayashi, M. R. Popovic, and K. Masani, "Method to reduce muscle fatigue during transcutaneous neuromuscular electrical stimulation in major knee and ankle muscle groups," *Neurorehabil. Neural Repair*, vol. 29, no. 8, pp. 722–733, Dec. 2015.

[14] M. Laubacher, A. E. Aksöz, R. Riener, S. Binder-Macleod, and K. J. Hunt, "Power output and fatigue properties using spatially distributed sequential stimulation in a dynamic knee extension task," *Eur. J. Appl. Physiol.*, vol. 117, no. 9, pp. 1787–1798, Sep. 2017.

[15] M. J. Wiest, A. J. Bergquist, M. G. Heffernan, M. Popovic, and K. Masani, "Fatigue and discomfort during spatially distributed sequential stimulation of tibialis anterior," *IEEE Trans. Neural Syst. Rehabil. Eng.*, vol. 27, no. 8, pp. 1566–1573, Aug. 2019.

[16] M. Laubacher *et al.*, "Stimulation of paralysed quadriceps muscles with sequentially and spatially distributed electrodes during dynamic knee extension," *J. NeuroEng. Rehabil.*, vol. 16, no. 1, pp. 1–12, Dec. 2019.

[17] M. Laubacher, E. A. Aksöz, S. Binder-Macleod, and K. J. Hunt, "Comparison of proximally versus distally placed spatially distributed sequential stimulation electrodes in a dynamic knee extension task," *Eur. J. Transl. Myol.*, vol. 26, no. 2, pp. 110–115, Jun. 2016.

[18] H. Zhou, Y. Wang, W. Chen, N. Zhang, L. Krundel, and G. Li, "Spatially distributed sequential array stimulation of tibial anterior muscle for foot drop correction," in *Proc. 37th Annu. Int. Conf. IEEE Eng. Med. Biol. Soc. (EMBC)*, Aug. 2015, pp. 3407–3410.

[19] S. Gabriel, R. W. Lau, and C. Gabriel, "The dielectric properties of biological tissues: III. Parametric models for the dielectric spectrum of tissues," *Phys. Med. Biol.*, vol. 41, no. 11, pp. 2271–2293, 1996.

[20] A. Kuhn, T. Keller, M. Lawrence, and M. Morari, "A model for transcutaneous current stimulation: Simulations and experiments," *Med. Biol. Eng. Comput.*, vol. 47, no. 3, pp. 279–289, 2009.

[21] P. B. Yoo, M. Sahin, and D. M. Durand, "Selective stimulation of the canine hypoglossal nerve using a multi-contact cuff electrode," *Ann. Biomed. Eng.*, vol. 32, no. 4, pp. 511–519, Apr. 2004.

[22] G. B. Saturnino, A. Antunes, and A. Thielscher, "On the importance of electrode parameters for shaping electric field patterns generated by tDCS," *NeuroImage*, vol. 120, pp. 25–35, Oct. 2015.

[23] D. R. McNeal, "Analysis of a model for excitation of myelinated nerve," *IEEE Trans. Biomed. Eng.*, vol. BME-23, no. 4, pp. 329–337, Jul. 1976.

[24] F. Rattay, "Analysis of models for extracellular fiber stimulation," *IEEE Trans. Biomed. Eng.*, vol. 36, no. 7, pp. 676–682, Jul. 1989.

[25] F. Rattay, "Analysis of models for external stimulation of axons," *IEEE Trans. Biomed. Eng.*, vol. BME-33, no. 10, pp. 974–977, Oct. 1986.

[26] M. J. Wiest, A. J. Bergquist, M. G. Heffernan, M. Popovic, and K. Masani, "Fatigue and discomfort during spatially distributed sequential stimulation of tibialis anterior," *IEEE Trans. Neural Syst. Rehabil. Eng.*, vol. 27, no. 8, pp. 1566–1573, Aug. 2019, doi: 10.1109/TNSRE.2019.2923117.

[27] A. Wongsarnpigoon and W. M. Grill, "Computational modeling of epidural cortical stimulation," *J. Neural Eng.*, vol. 5, no. 4, pp. 443–454, Dec. 2008.